Heliyon 10 (2024) e31107

Contents lists available at ScienceDirect

Heliyon

journal homepage: www.cell.com/heliyon

Research article

3D printing for energy optimization of building envelope – Experimental results

Tullio de Rubeis [a,*], Annamaria Ciccozzi [b], Domenica Paoletti [b], Dario Ambrosini [b]

[a] Department of Civil, Construction-Architectural and Environmental Engineering (DICEAA), University of L'Aquila, L'Aquila, Italy
[b] Department of Industrial and Information Engineering and Economics (DIIIE), University of L'Aquila, L'Aquila, Italy

ARTICLE INFO

Keywords:
3D printing
Heat transfer
Thermal analysis
Experimental analysis
Hot box
Energy efficiency

ABSTRACT

The building sector is a major contributor to the world's energy consumption, exhibiting an ever-increasing trend. Heat losses through the building envelope constitute the most significant factor. Furthermore, the construction process has seen limited technological advancements in recent years, remaining heavily reliant on manual labor. Additive manufacturing emerges as a promising approach, with applications in the building sector on the rise. However, research on the thermal performance of 3D-printed components remains limited. Despite its recent introduction in the construction industry, 3D printing has yet to attain a level of maturity commensurate with other established methods.

This paper aims to reduce this gap by analyzing 3D-printed blocks from a heat transfer perspective. The article introduces two key innovations. Firstly, it explores the design of various internal geometries and air gaps aimed at minimizing heat flux exchange between block surfaces. Secondly, it presents an experimental study conducted with a custom-designed setup tailored for testing 3D printed blocks. The blocks are constructed using recyclable plastic material and feature different internal geometries based on hexagonal cells. While the plan size of the cells remains consistent, their vertical structures vary as follows: 1) Block 1: Hexagonal air cavities without horizontal partitions. 2) Block 2: Hexagonal air cavities with three horizontal partitions, dividing the cells vertically into four parts. 3) Block 3: Honeycomb structure characterized by three horizontal partitions and staggering along the vertical axis.

Their performance was experimentally evaluated using the Hot Box method, heat flow meter sensors, and infrared thermography. The results demonstrated reductions of up to 11.5 % in terms of thermal transmittance (U-value) with the inclusion of horizontal partitions. Starting from a U-value of 1.22 ± 0.04 W/m^{2}K (Block 1), a transmittance of 1.08 ± 0.04 W/m^{2}K was achieved for the honeycomb structure with horizontal partitions (Block 3).

1. Introduction

The construction industry stands as one of the largest energy consumers, responsible for approximately 40 % of energy consumption and 36 % of greenhouse gas (GHG) emissions in the European Union (EU) [1]. These emissions stem primarily from the construction process, building usage, renovation, and demolition [1]. Consequently, enhancing the energy efficiency of buildings and integrating renewable energy sources are paramount to achieving the ambitious goal of carbon neutrality by 2050, as outlined in the

* Corresponding author.
E-mail address: tullio.derubeis@univaq.it (T. de Rubeis).

https://doi.org/10.1016/j.heliyon.2024.e31107
Received 26 March 2024; Received in revised form 8 May 2024; Accepted 9 May 2024
Available online 10 May 2024

European Green Deal [2,3]. At present, about 75 % of buildings in the EU exhibit inadequate energy efficiency, necessitating interventions in existing structures [1]. Renovating existing buildings holds significant potential, with the prospect of decreasing overall EU energy usage by 5–6% and slashing carbon dioxide emissions by roughly 5 % [1]. Therefore, fostering expertise in designing innovative solutions and employing energy-efficient materials is crucial. The pursuit of increasingly complex and high-performance buildings must be paralleled by the advancement of innovative and efficient construction methods.

The construction sector is often regarded as a low-tech industry, with technological progress lagging behind other sectors in recent years [4]. Consequently, there is a clear need for innovation in construction processes. Additive manufacturing (AM) has the potential to bridge the gap between traditional construction methods and customized solutions [5]. 3D printing (3DP) enables highly automated manufacturing processes by sequentially depositing materials based on digital files [6,7]. Moreover, the possibility of realizing highly optimized solutions in terms of construction time, geometries customization, lack of waste materials, and reduced costs make 3DP a potential technology of the future [8–10].

1.1. Building envelope and its optimization

Limiting the energy consumption of buildings often involves optimizing the building envelope, a key contributor to heat losses. Designing high-performance enclosures can significantly reduce the energy consumed by heating and cooling systems. Various approaches can enhance the thermal behavior of building envelopes, including the use of high-performance insulating materials and structural improvements to external envelopes [11].

One effective strategy for improving the thermal performance of building envelopes is the incorporation of air cavities, a method widely adopted to enhance thermal resistance. Numerous studies, employing either experimental or numerical simulations, have investigated heat transfer in air cavities with diverse shapes and configurations. For example, Lorente et al. [12] developed a simplified analytical model of thermal behavior (conduction, convection, and radiative transfer) for vertical cavities with a high height-to-thickness ratio, as well as a series of cavities arranged in a row. Stefanizzi et al. [13] examined the common geometry of blocks characterized by horizontal and vertical perforations, considering various mean temperatures and temperature differences across surfaces perpendicular to the heat flux direction. Their research revealed that relying on standards to estimate the thermal resistance of air cavities could lead to significant errors in certain geometric configurations and boundary conditions. For instance, in the case of cavities within hollow brick blocks with horizontal perforations, thermal resistance could be underestimated by up to 40 %.

Hu et al. [14] explored how the thermal behavior of blocks would be affected if some cavities were filled with insulating material. They fabricated six groups of block models with varying filling positions and rates to determine the optimal filling position and rate for composite self-insulation hollow blocks.

Recent studies have underscored the critical role of cavity geometry within building blocks in shaping the thermal performance of the building envelope. Al-Tamimi et al. [15] employed finite element modeling (FEM) to pinpoint the most effective cavity geometry for reducing thermal heat flow in masonry concrete blocks. Experimental findings demonstrated that the newly designed block with optimized geometry, devoid of any insulating materials, achieved a remarkable thermal insulation improvement of up to 71 % compared to other models, including those currently available on the market. Similarly, Suntharalingam et al. [16] utilized FEMs to compare various samples of concrete walls, assessing the thermal properties offered by different geometric configurations. The study concluded that walls featuring multiple rows of cavities and internal partitions exhibit significantly enhanced performance.

Honeycomb structures, inspired by the geometric arrangement of bee honeycombs, have gained significant traction across diverse fields, including architecture [17]. Renowned for their effectiveness in energy applications, honeycomb structures serve as optimal thermal barriers and heat sinks [18]. In this context, Zhu et al. [19] analyzed the heat transfer mechanism in cement-based honeycomb structures (CHSs) using infrared thermal imaging technology. Their study revealed that thermal diffusion weakens layer by layer upward through the honeycomb cavities. However, a major challenge in this field lies in comprehending the unique properties of honeycomb structures, which are influenced by their geometric configurations, scales, and the materials utilized [17].

Hence, it seems evident that the search for useful geometric solutions to minimize heat transfer across opposing faces of a block is widely debated in the literature. However, contemporary construction technologies limit the shapes of building blocks to simplistic geometries, seldom optimized for thermal efficiency. Within this framework, emerging and still little-explored 3DP can be an optimal approach for exploring novel configurations of the building envelope to enhance thermal performance, thanks to its capacity to fabricate intricate geometries. Examples of using AM to create thermal blocks are still few, although they are rapidly increasing. For example, de Rubeis [20] demonstrated the potential of AM for insulating systems by investigating the thermal performance of a 3D-printed polylactic acid (PLA) hollow block through theoretical and experimental analyses. The block's internal cavities were subsequently filled with various waste materials, such as polystyrene and wool, to assess the impact of insulation materials on the thermal performance of the hollow blocks. In subsequent studies, de Rubeis et al. [18] conducted theoretical and experimental analyses to investigate the thermal behavior of three PLA-printed blocks with varying internal geometries: (i) multi-row structure, (ii) square structure, and (iii) honeycomb structure. The findings revealed that hexagonal cells exhibited higher efficiency, indicating that increasing the complexity of the internal structure led to a reduction in heat flow. Building upon this research, de Rubeis et al. [21] further explored the hexagonal cell block with cavities filled with various natural and recyclable waste-insulating materials. The results demonstrated that the incorporation of waste material significantly enhanced the thermal performance of the 3D-printed block, achieving a reduction of up to 57 % in terms of thermal transmittance.

1.2. Paper contribution

This work builds upon the findings discussed in a previous paper [22] by investigating the potential of 3DP in optimizing the energy performance of the building envelope.

The primary innovations of this study encompass two key aspects:

i) Exploring the utilization of 3DP to fabricate blocks with internal geometries engineered to minimize heat transfer between opposing faces, such as those of a wall.
ii) Establishing an appropriate experimental framework to assess the thermal performance of 3D printed blocks.

The primary objective is to comprehensively understand and quantify how the thermal performance of blocks with hexagonal air cavities varies with changes in internal geometries.

The study examines three blocks characterized by different internal configurations: 1) Block 1 with hexagonal air cavities but no horizontal partitions; 2) Block 2 with hexagonal air cavities and three horizontal partitions dividing the cells vertically into four parts; and 3) Block 3 with a honeycomb structure featuring three horizontal partitions and staggering along the vertical axis.

The rationale for this study is grounded in theoretical knowledge indicating that the arrangement of air cavities within the block significantly influences its heat transfer, primarily through convective heat transfer mechanisms. Building upon the analysis of Block 1, which was experimentally examined with air cavities arranged vertically (Block 1a) and then adjusted by 90° (Block 1b), Blocks 2 and 3 were designed.

Experimental analysis, conducted using the Hot Box method, Heat Flux Meter (HFM), and Infrared Thermography (IRT) technique, enabled quantification of the effects of internal geometries on the thermal transmittance of the blocks.

The paper is structured into five sections as follows: Section 2 provides a summary of related works analyzed in the literature; Section 3 outlines the methodology employed, including the design and construction of the blocks, and details the experimental phases. Section 4 presents and discusses the results. Finally, Section 5 summarizes the main findings of the study.

Table 1
Summary of the works that analyzed the thermal performance of 3D-printed components.

Reference	Year	Research objective	Experimental approach	Thermal parameters	Results
[23]	2018	Adaptive facade panel	Heat flux; Hot-Box	λ (W/mK)	$0.09 < \lambda < 0.1$
[24]	2021	3D-printed plates	IRT; Numerical modeling	T (°C)	$36 \leq T_1 \leq 55$ (front) $32 \leq T_2 \leq 50$ (back)
[25]	2020	Multilayer insulation with quadrangle, hexagonal, and triangle closures	Poensgen apparatus	λ (W/mK)	$0.06 < \lambda < 2.5$
[26]	2023	3D-printed concrete and hollow slabs with and without insulation material	Heat Flux; Hot-Box; IRT	T_{si} (°C)	$T_{s,int,1} = 48$ (two cavities) $T_{s,int,2} = 49$ (three cavities)
[27]	2018	3D-printed concrete wall	Hot Plate Apparatus	R (m^2K/W); U (W/m^2K)	$R = 5.45$ $U = 0.18$
[28]	2020	3D-printed wall	Numerical modeling	U (W/m^2K)	$0.15 < U < 0.55$
[29]	2021	3D-printed concrete walls with cavities	Heat flux; Hot-Box; Numerical analysis	λ (W/mK)	From $\lambda_1 = 0.37$ To $\lambda_2 = 1.1$
[30]	2022	3D-printed enclosing structures	Hot Box; IRT; Numerical modeling	U (W/m^2K)	$U = 1.18$
[31]	2021	32 3D-printed walls	Numerical modeling	U (W/m^2K)	$0.34 < U < 3.16$
[32]	2023	7 3D-printed walls	Numerical modeling	λ (W/mK); U (W/m^2K); T (°C)	$0.586 \leq U_1 \leq 0.828$ $0.199 \leq U_2 \leq 0.578$
[33]	2020	Modular 3D-printed vertical green wall	Numerical modeling	Q (W/m^2)	$Q = 3.94$
[34]	2021	3D-printed block	Numerical modeling	U (W/m^2K)	$U = 0.94$
[20]	2022	3D-printed blocks	Heat Flux; Hot-box; IRT	U (W/m^2K)	$U_1 = 2.19$ $U_2 = 1.24$ $U_3 = 0.69$
[18]	2022	3D-printed blocks	Heat Flux; Hot-box; IRT; Numerical modeling	U (W/m^2K)	$U_1 = 1.43$ $U_2 = 1.25$ $U_3 = 1.22$
[21]	2023	3D-printed blocks	Heat Flux; Hot-box; IRT	U (W/m^2K)	$U_1 = 1.22$ $U_2 = 0.65$ $U_3 = 0.53$ $U_3 = 0,66$

Legend. λ: Thermal Conductivity. IRT: Infrared thermography. T: Temperature. $T_{s,int}$: Internal surface temperature. R: Thermal resistance. U: Thermal transmittance. Q: Heat flux.

2. Related works

In recent years, numerous studies have delved into the potential of 3DP to optimize the thermal performance of building envelopes through topology. Sarakinioti et al. [23] developed a façade panel integrating insulating properties with heat storage in a complex, mono-material geometry created with 3DP. Mihalache et al. [24] investigated the impact of intricate internal wall structures on thermal performance to prevent overheating induced by thermal radiation. Grabowska and Kasperski [25] proposed the use of 3DP to produce prototype insulating materials from plastic. They designed and printed multi-layer materials with quadrangle, hexagonal, and triangle closures. Subsequently, they developed a mathematical model and experimentally validated it to determine the most efficient configuration. Dey et al. [26] analyzed the thermal performance of 3D-printed concrete slabs potentially used as walls. The slabs were designed hollow to allow the insertion of insulating material inside them. Kaszynka et al. [27] compared the attributes of conventional walls to those of 3D-printed walls. Their findings illustrated that the undulating structure of the 3D-printed walls enhanced mortar adhesion, promoting the effective attachment of thermal insulation. Alkhalidi et al. [28] designed distinct printable wall

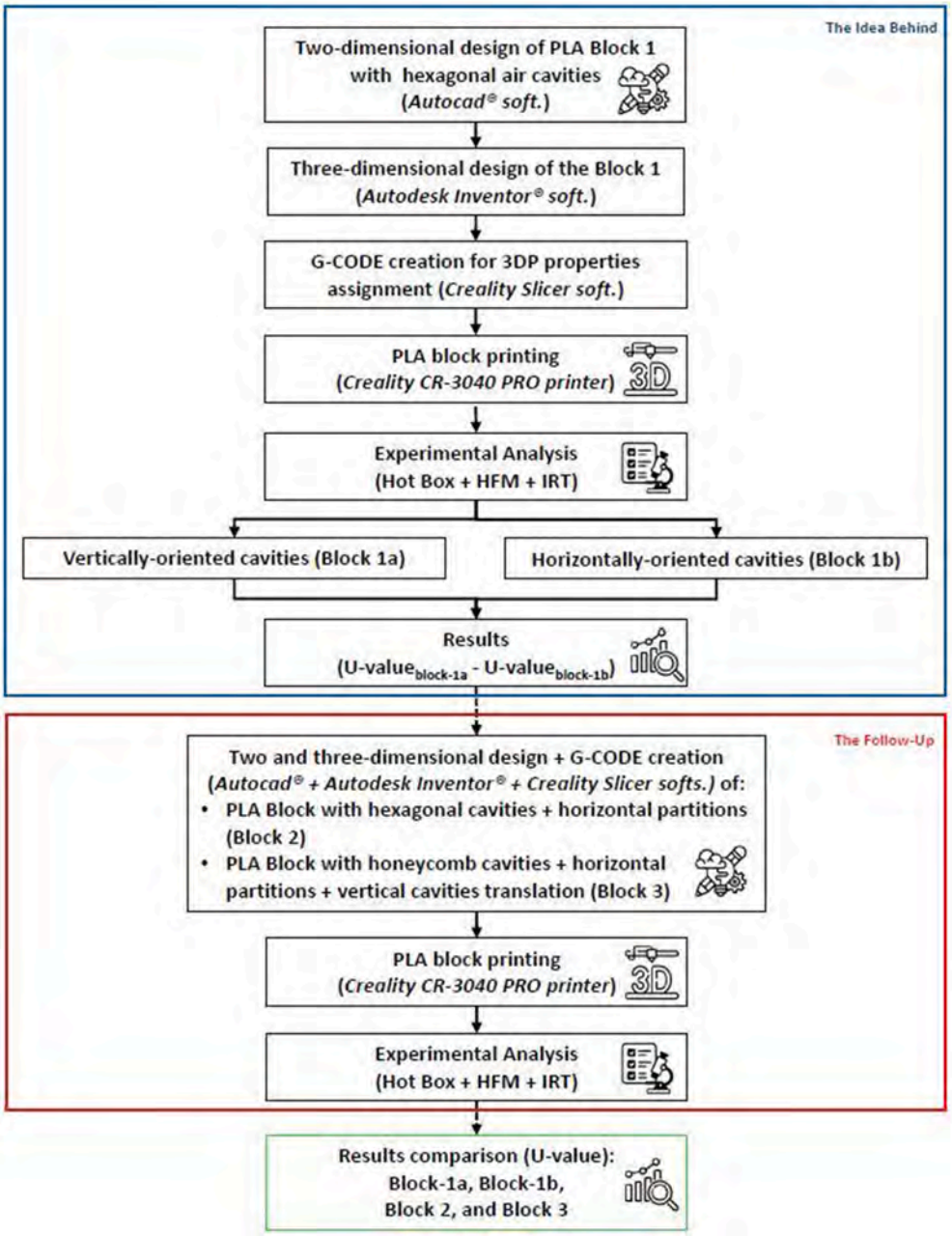

Fig. 1. Methodology flowchart.

configurations with different materials to reduce U-values of painted walls, aligning with regulations specific to climatic zones. Strategies for thermal improvement of cavity arrangement in 3D-printed concrete façade elements are presented through the analysis of two 3D-printed cement-based façade construction materials, distinguished by density and thermal conductivity [29]. Maraias et al. [29] discovered that the choice of wall geometry depends on the printing material.

Similarly, Nemova et al. [30] conducted theoretical and experimental investigations to assess the thermal efficiency of 3D-printed concrete (3DPC) envelopes featuring different configurations, material arrangements, and insulation types. Suntharalingam et al. [31] and Cuevas et al. [32] studied different topological wall variants to identify the most energy-efficient configurations. In particular, they analyzed 32 configurations with and without different insulating materials. Cuevas et al. [32] investigated 7 configurations using two different cement mixtures. He et al. [33] designed a prototype building envelope, the 3D-VtGW, consisting of 3D-printed modular elements serving as the backbone for a green wall system to improve the energy efficiency of the building. El-Mahdy et al. [34] created a prototype 3D-printed block, the SaltBlock, to encourage designers to explore AM techniques by testing their actual applicability in the construction sector.

In this context, a research line initiated by de Rubeis [20] and extended by de Rubeis et al. [18,21] centers on the investigation of 3D-printed block prototypes for thermal optimization of the building envelope. Specifically, the thermal properties of the samples were examined by altering their geometric configurations [18], with some cases hypothesizing the insertion of insulating material inside the cavities of the blocks [20,21].

Table 1 provides a summary of the primary findings from the related works discussed.

3. Methodology

The methodology employed in this study builds upon considerations discussed in previous studies [18,20–22], where the effects of different air cavity geometries on the thermal performance of 3D-printed blocks were examined. These prior articles demonstrated that the hexagonal geometry consistently yielded the best thermal transmittance values.

Based on these findings, the current work initially investigated a block featuring hexagonal air cavity geometry, first oriented vertically and then horizontally (as illustrated in "The Idea Behind" in Fig. 1). Subsequently, based on the obtained results, a block with hexagonal cavities and horizontal partitions was designed. Finally, a final block configuration was developed, characterized by a honeycomb structure, horizontal partitions, and vertical translation of cavities. In designing the different blocks, we kept the volume of air contained in the cavities constant, but made changes to their shape and arrangement. The thickness of the printing material and the number of air cavities were also kept constant for all the blocks produced.

From the executive point of view, the methodology employed can be divided into three phases:

- **Design Phase**: Designing the blocks in both two and three dimensions using *Autocad*® and *Autodesk Inventor*® software, where shapes and dimensions were defined based on the printer's capabilities.
- **Construction Phase**: Generating G-Code using *Creality Slicer* software to assign printing properties and printing the blocks with the *Creality CR-3040 PRO* printer (Shenzen Creality 3D Technology Co., Ltd., Shenzhen, China) using the Fused Deposition Modeling (FDM) technique. PLA was selected as the printing material due to its properties, cost-effectiveness, and environmentally friendly, biodegradable nature [35–37].
- **Experimental Phase**: Conducting experimental studies using the Hot Box equipped with heat flux sensors and temperature probes to study the thermal performance of the blocks. Furthermore, the surface thermal distribution of the blocks was evaluated using the IRT technique.

The illustration of the methodology used in this work is shown in Fig. 1.

3.1. Theoretical background

Heat transfer in the blocks is not simple to model. Basically, we are dealing with a series of cavities heated from the side; however, in some geometries, internal cavities could also experience heating from the top and the bottom. Considering a single enclosure, we can identify the following contributions to the heat flux:

- Heat conduction through the PLA walls.

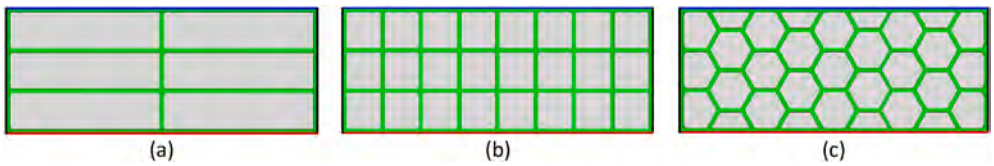

Fig. 2. 3D printed blocks [18]. (a) Multi-row structure. (b) Square structure. (c) Honeycomb structure. Legend: (Blue) is the outer surface, (Red) is the inner surface, (Green) is the PLA, (Grey) is the air, and (Black) the adiabatic surfaces. (For interpretation of the references to colour in this figure legend, the reader is referred to the Web version of this article.)

- Convective heat transfer through air.
- Radiation heat transfer through air.

Focusing on the heat transfer phenomenon, some hints could be obtained about the improvements of the isolating features of the blocks, i.e. about how to reduce their U-values.

3.1.1. *Heat conduction through the PLA walls*

Generally speaking, increasing the geometric complexity of the structure increases the effective path the heat has to travel by conduction, thus increasing the thermal resistance.

This idea can be illustrated by considering Fig. 2, showing examples of blocks with increasingly complex geometry; as heat conduction is along the walls (in green), the blocks exhibit increasingly effective conductive paths.

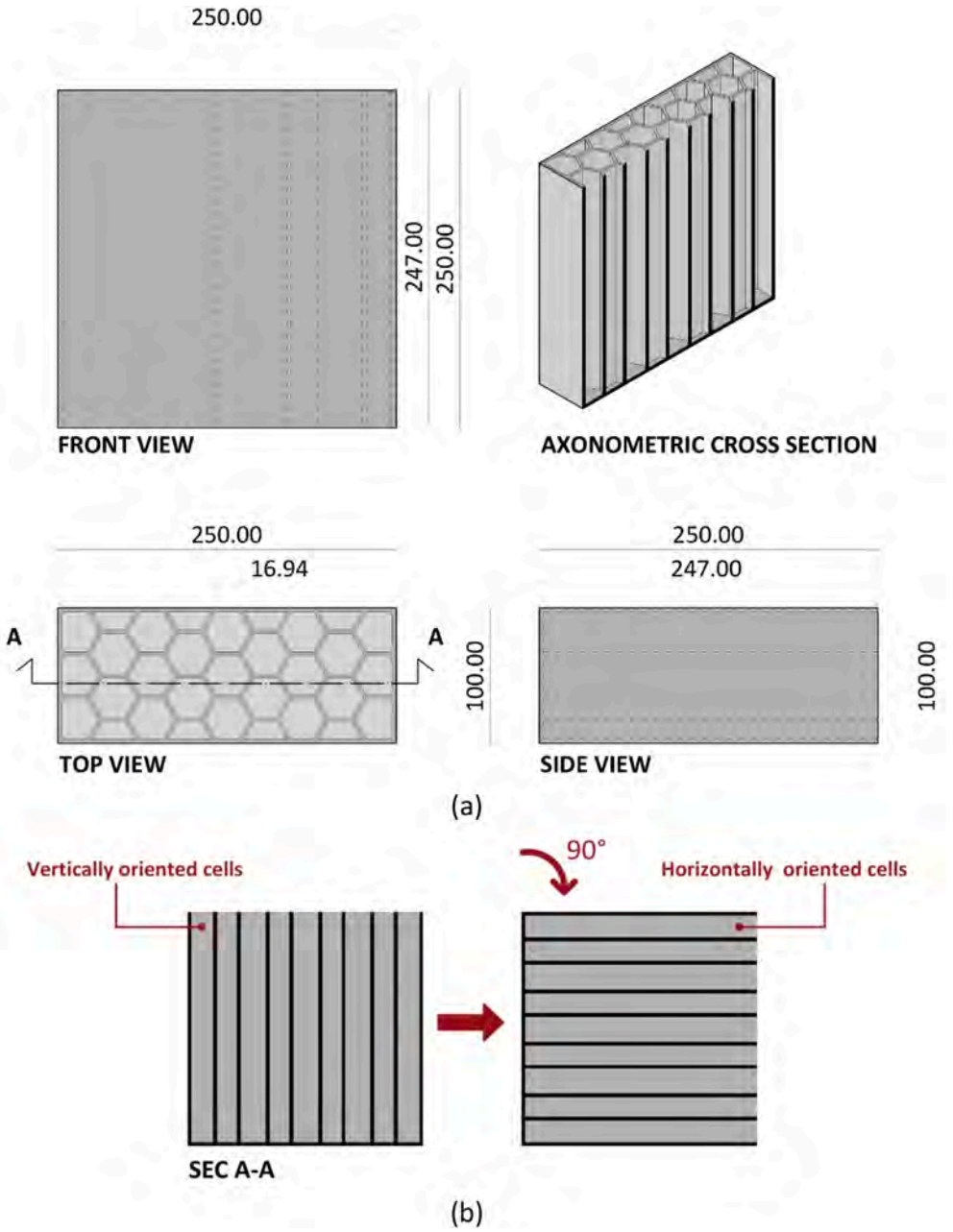

Fig. 3. Block 1 with hexagonal cells and no horizontal partitioning. (a) 2D and 3D Block designs. (Measurements in millimeters). PLA thickness is equal to 3 mm. (b) The two configurations tested for the block: vertical and horizontal cell orientation.

3.1.2. Convective heat transfer through air

The convective heat flux $\dot{q}_c$ in an enclosure can be written as a function of an "effective conductivity" (λ_{eff}), as shown by Eq. (1) [38].

$$\lambda_{eff} = \lambda \cdot Nu \tag{1}$$

Therefore, the convective heat flux, which considers both conduction and convection, is provided by Eq. (2) [38].

$$\dot{q}_{conv} = \lambda_{eff} \cdot Nu \cdot \frac{\Delta T}{L} = \lambda \cdot Nu \cdot \frac{\Delta T}{L} \tag{2}$$

where λ is the thermal conductivity of air, ΔT is the temperature difference between the hot and cold surfaces of the enclosure, and L is the dimension of the cavity in the main direction of the flow. The Nusselt number (*Nu*) can be determined from various correlations depending on the aspect ratio, orientation, and direction of the heat flow [38].

The enclosure isolates at its best in the pure conduction state, i.e. when $Nu = 1$. *Nu* is generally related to the Prandtl number Pr (depending on the fluid), the Rayleigh number Ra_L, and the aspect ratio H/L (ratio of the enclosure height H and the distance L between hot and cold surfaces).

The Rayleigh number in cavities is based on the enclosure height [39], as shown by Eq. (3).

$$Ra_H = \frac{g \cdot \beta \cdot (T_h - T_c) \cdot H^3}{\alpha \nu} \tag{3}$$

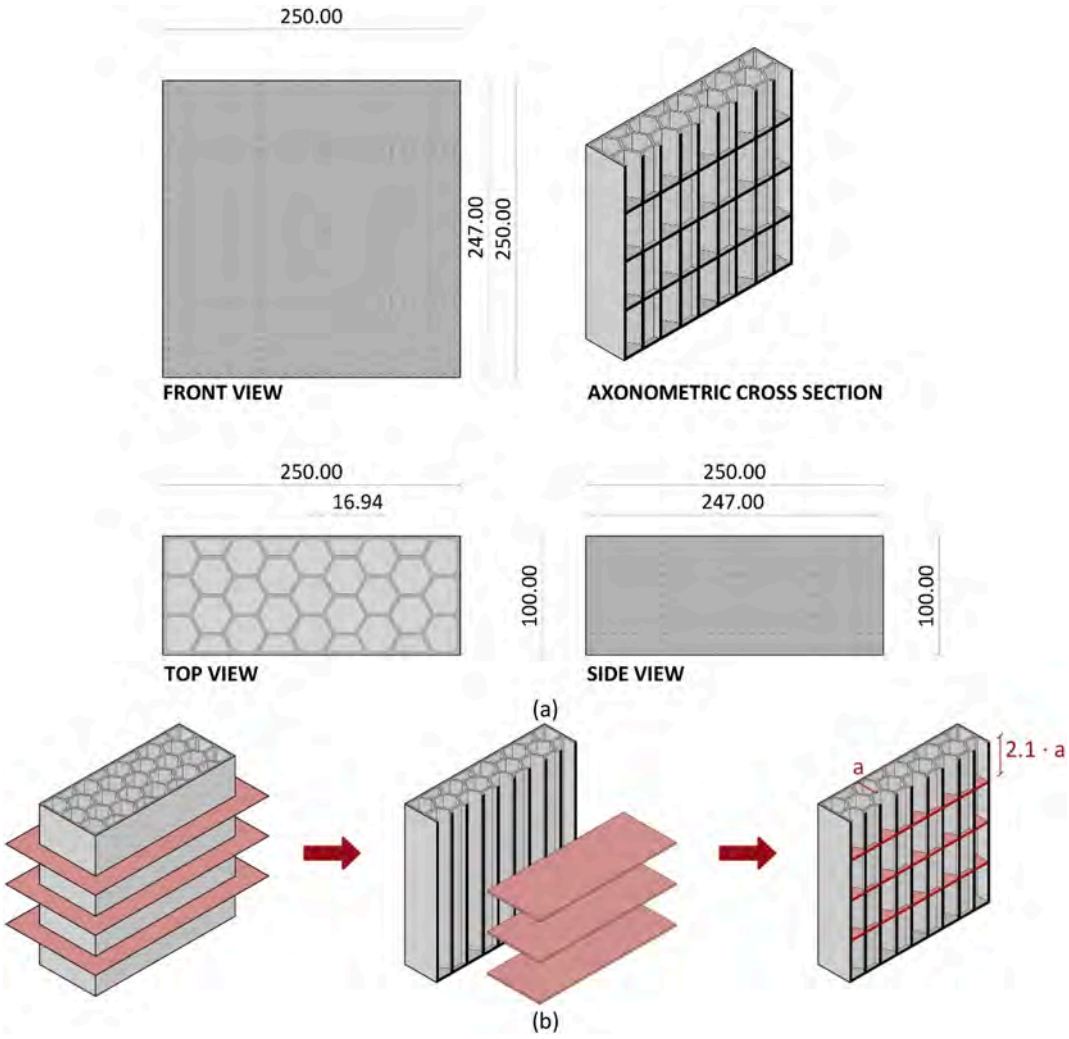

Fig. 4. Block 2 with hexagonal cells and three horizontal partitions. (a) 2D and 3D Block designs. (Measurements in millimeters). PLA thickness is equal to 3 mm. (b) Placement of horizontal partitions.

where g is the gravitational acceleration, α is the thermal diffusivity, β is the coefficient of volume expansion, T_h is the temperature of the hot surface, T_c is the temperature of the cold surface, H is the characteristic length of the geometry, ν is the kinematic viscosity of the fluid.

Moreover, *Nu* depends also on the aspect ratio H/L. Bejan [39] summarized several correlations for two-dimensional enclosure heated from the side by plotting the Nusselt number *Nu* as a function of the ratio L/H.

Previous considerations are valid for singular enclosures. When cavities are grouped in a multicellular structure, there is heat transfer between cells.

3.1.3. Radiation heat transfer

Heat transfer by radiation in the cavities, depending on temperature and emissivities of the internal surfaces and the view factors, is not simple to model. As a basic approach, we may observe that planes parallel to the hot and cold surfaces (see Fig. 2) act as radiation shields. Therefore, a simple way to reduce the contribution to the heat flux could be the insertion of surfaces opaque to the radiation.

3.2. Design phase

In this section, the process of designing the blocks in both two and three dimensions is explained, along with the rationale behind the decisions made and the dimensional constraints considered. Specifically, all blocks have the same size (250 mm × 250 mm x 100 mm - width x height x depth), which is dictated by the dimensional limitations of the 3D printer.

3.2.1. Block 1: hexagonal cell block

Block 1, which incorporates hexagonal cells without horizontal partitions (Fig. 3a), was subjected to examination with both vertical and horizontal cell orientations (i.e., rotated by 90°), as illustrated in Fig. 3b. The rationale for this rotation is linked to its influence on convective heat transfer. According to heat transfer theory, such rotation should mitigate convective heat transfer effects, especially if the air cavities tend to contract [39].

The block cavities, arranged in three rows, are characterized by sides of 16.9 mm and a height of 247.0 mm.

3.2.2. Block 2: hexagonal cell block with horizontal partitions

The design of Block 2 originates from the fundamental configuration of Block 1, featuring a hexagonal geometry of air cavities (see Fig. 4a). However, three horizontal partitions were introduced, dividing the block vertically into four equal sections (see Fig. 4b). Specifically, the partitions were inserted to ensure that the proportions of the cavities adhered to those of a real honeycomb cell, where the height is approximately 2.5 times its width [40]. Therefore, starting from the size of the cell opening ("*a*" in Fig. 4b), the partitions were inserted at a distance ($x \bullet a$). This ensured that all cavities had the same height, closely approximating the dimension ($2.5 \bullet a$). Considering that "*a*" is equal to 29 mm, the aforementioned partitions were placed at a distance of ($2.1 \bullet a$) from each other. This arrangement resulted in four vertical rows of cells, all of equal height, measuring 59.5 mm.

3.2.3. Block 3: the honeycomb structure

Inspired by the intricate structure of honeycombs, the design of this block draws upon the mathematical principles elucidated by Polachek [40]. In recent years, the quest for architectural solutions inspired by nature has burgeoned, with AM enabling us to push the boundaries of construction further. Biomimetic architecture has found application in thermal design, as evidenced by Andréen and Soar's research on the thermal properties of termite mounds [41].

The construction technique of a honeycomb is such that it is possible to keep the volume of the cells unchanged by reducing their surface area. Therefore, bees use less wax to obtain the same honey volume. Moreover, the cells of honeycombs are translated to each other for structural integrity (Fig. 5).

In light of these considerations, the honeycomb structure has been reconfigured to emulate a condition like that analyzed for the hexagonal cells with horizontal partitions, as seen in Block 2. Fig. 6 illustrates the honeycomb structure designed for Block 3.

As previously described, a honeycomb makes it possible to reduce the surface area of material while keeping the volume

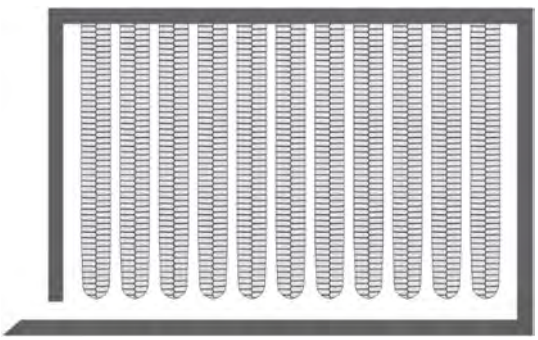

Fig. 5. Longitudinal section of the honeycombs in a hive. Adapted from Ref. [42].

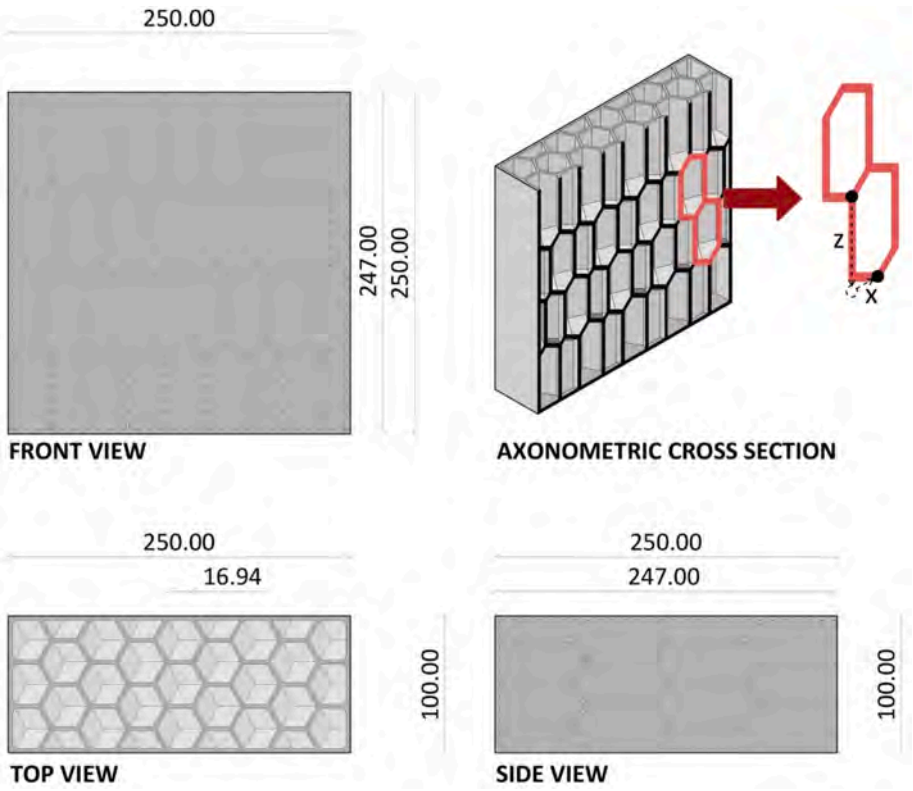

Fig. 6. Block 3 with a honeycomb structure of the cells, horizontal partitions, and translation of the cells. (Measurements in millimeters). PLA thickness is equal to 3 mm.

unchanged. This feature is attributed to geometric principles. Beginning with a cell featuring a hexagonal base (an eight-sided prism, as depicted in Fig. 7a), three pyramidal volumes are subtracted from the lower end (highlighted as red pyramids in Fig. 7b). These subtracted volumes are then repositioned (red pyramids in Fig. 7c) to form a trihedral pyramid base at the lower end (ten-sided prism, as depicted in Fig. 7d).

To clarify the vertical translation of the cells, the three-dimensional schematic is provided in Fig. 8.

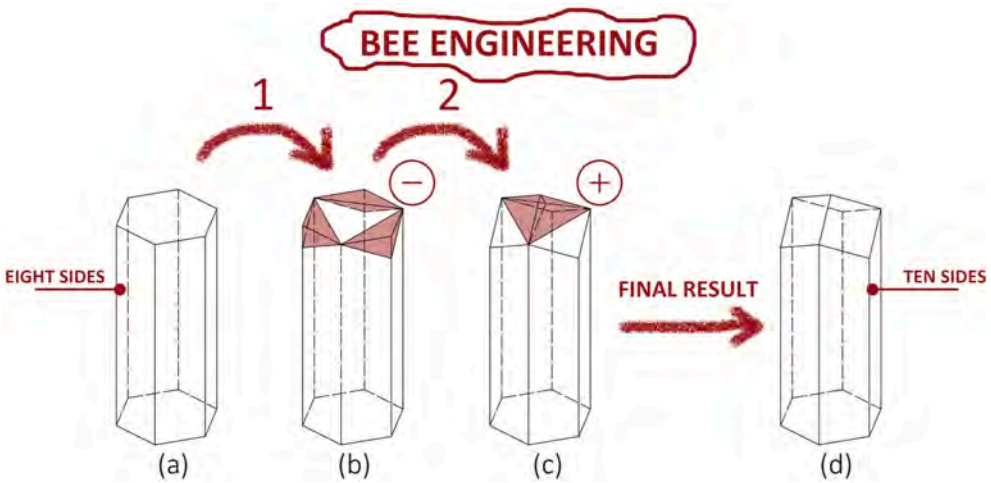

Fig. 7. The honeycomb cell design process.

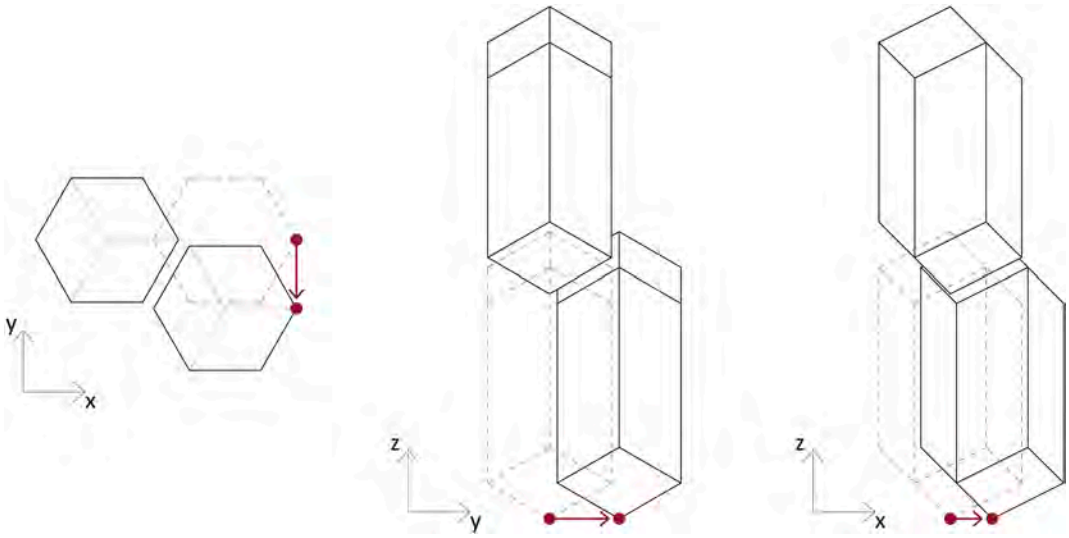

Fig. 8. Schematic of honeycomb cell fitting.

3.3. Construction phase

All blocks analyzed in this paper were constructed following the same procedure, which comprised three main steps. The initial step involved a three-dimensional design using *Autodesk Inventor*® software, enabling the depiction of air cavities and horizontal partitions. Fig. 9 illustrates the axonometric cross-sections of the three blocks.

The second step in the construction process involves configuring all printing properties using the *Creality Slicer* software. This includes assigning properties such as shell and filling characteristics, printing material, nozzle and print bed temperatures, printing speed, and nozzle size. All three blocks were manufactured using a brass nozzle with a diameter of 0.4 mm, operating at a temperature of 210 °C, ideal for melting PLA filaments. The print bed temperature was consistently maintained at 60 °C across all cases.

Among the other parameters that characterized the printing of the blocks, it is important to mention the width of the line, set to 0.44 mm, the thickness of the walls, set to 0.66 mm, the filling density, set to 5 %. The aforementioned parameters have been determined to ensure the right balance between material savings and block strength. The printing speed was set at 100 mm/s, while the filling speed was set at 10 mm/s to ensure that the material adhered well to the underlying layer.

Upon defining all printing parameters, the G-Code was generated (refer to Fig. 10).

The printing characteristics were communicated to the Creality CR-3040 PRO printer through the G-Code. Subsequently, the blocks were printed, as depicted in Fig. 11.

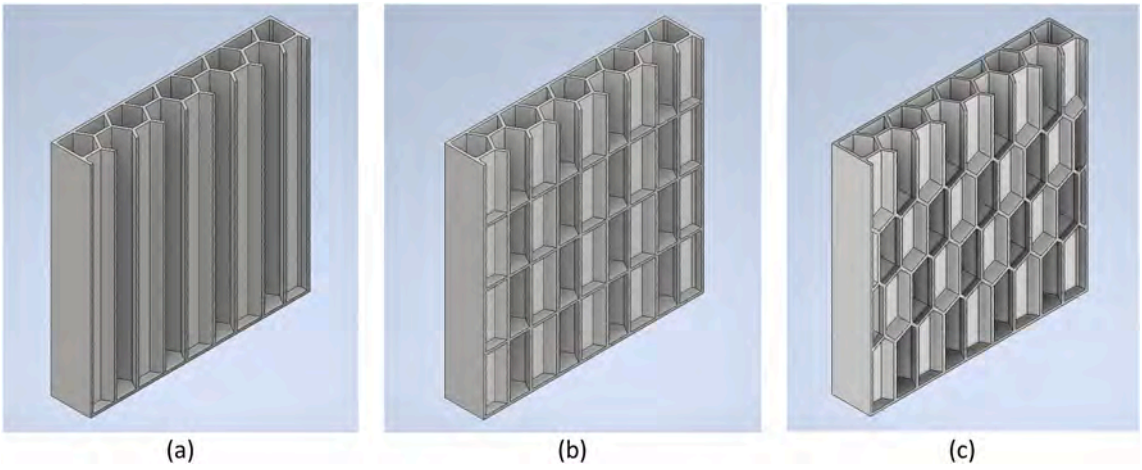

Fig. 9. Axonometric cross-sections of the three-dimensional models of the blocks. (a) Block 1. (b) Block 2. (c) Block 3.

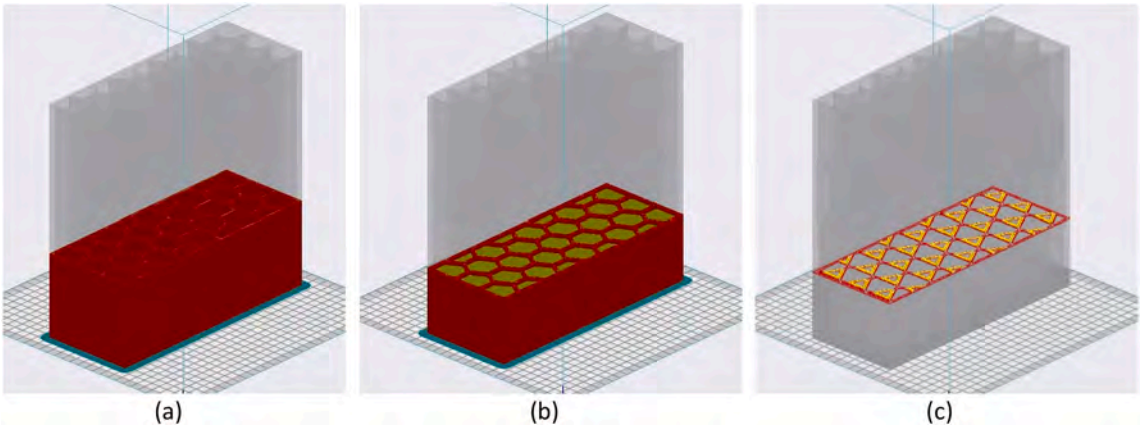

Fig. 10. The cross-sections of the block with the print layers visualization on Creality Slicer software. (a) Block 1. (b) Block 2. (c) Block 3.

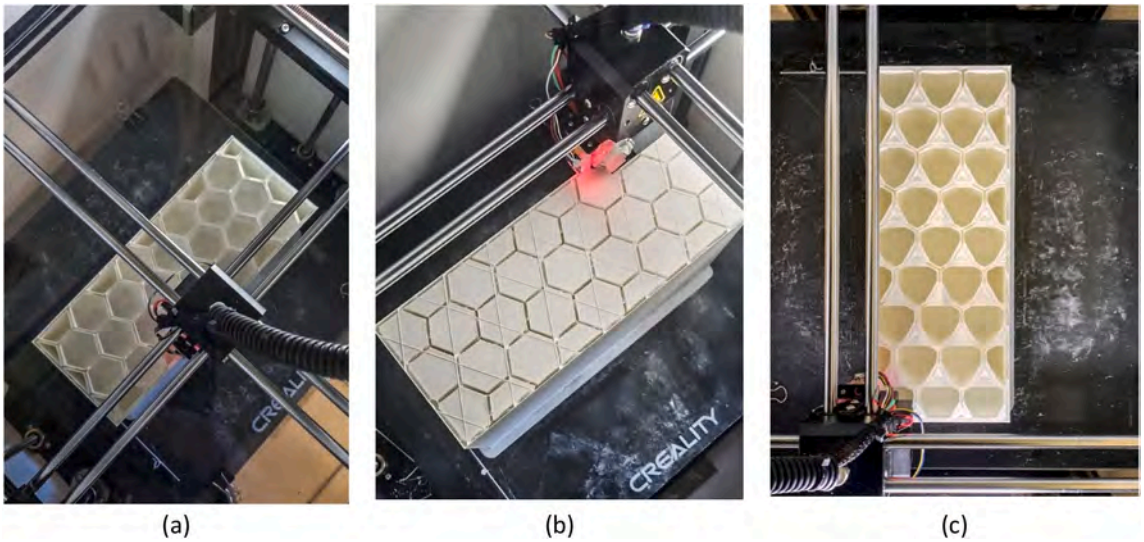

Fig. 11. Picture of the printing process. (a) Block 1. (b) Block 2. (b) Block 3.

3.4. Experimental phase

The experimental phase was conducted using a specially constructed Hot Box designed to meet the dimensional constraints of 3D-printed blocks, which are 250 mm × 250 mm (width x height). This Hot Box facilitated experimental campaigns under steady-state conditions, ensuring controlled and repeatable testing environments. A comprehensive explanation of the Hot Box design and implementation can be found in Ref. [20]. Fig. 12 presents a schematic representation of the employed Hot Box.

The experimental campaigns were carried out utilizing the HFM Method, which involves measuring heat flux and surface temperatures (both internal and external). The heat flux sensor was installed on the inner (hot) surface of the blocks, the surface temperatures were installed on both external sides of the blocks (inner and outer), and the temperature inside the Hot Box was monitored using an air temperature probe. Fig. 13 illustrates the experimental setup employed for these measurements.

The operating conditions of the experimental tests were imposed starting from the laboratory temperature (equal to 23 °C). The electric heater inside the Hot Box was set to achieve an internal block surface temperature of 46 °C, establishing a temperature difference of at least 20 °C, which is suitable for applications of the HFM method [43]. The sampling frequency was configured to 10 min. Each experimental test for every block lasted for a duration of 48 h, with the final 24 h considered for analysis, during which stable thermal conditions were achieved.

The heat flux and internal and external surface temperatures were processed using the progressive average method to determine the conductance (Λ) of the blocks, as outlined in Eq. (4). Subsequently, the thermal transmittance (U) was calculated by considering the surface thermal resistances specified by the ISO 6946 standard [44], with $(R_{s,int})$ equal to 0.13 m^2K/W and $(R_{s,ext})$ equal to 0.04 m^2K/W, as demonstrated in Eq. (5) [44].

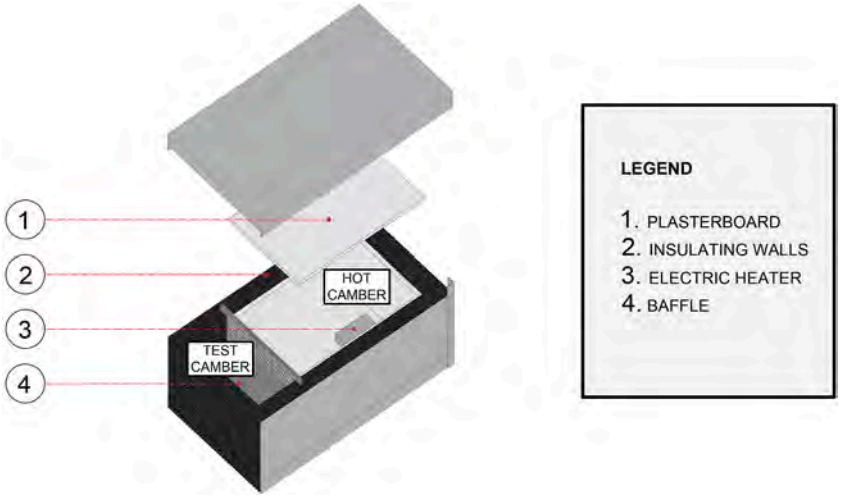

Fig. 12. Schematic of the Hot Box used for the experimental analyses.

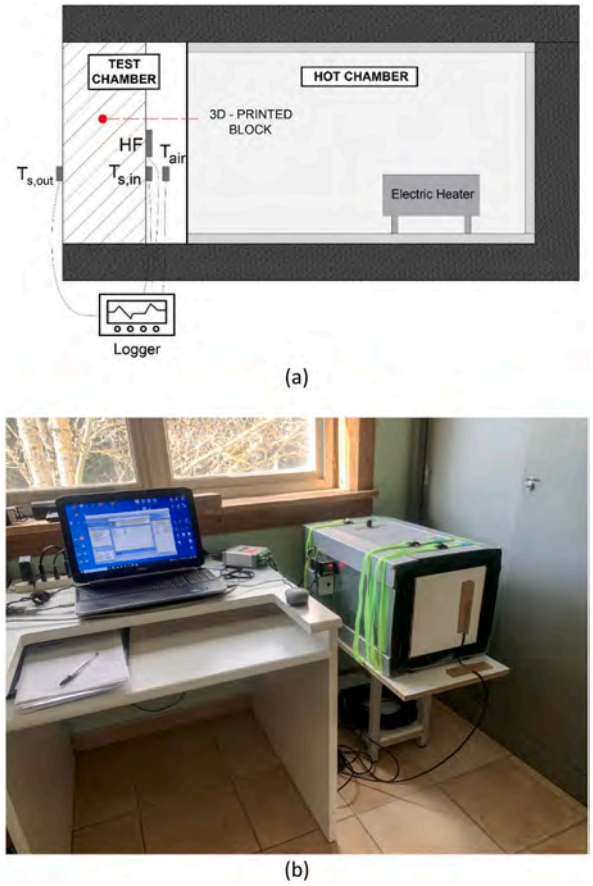

Fig. 13. The experimental setup. (a) Schematic of the measuring instruments employed. (b) Setup picture.

$$\Lambda = \frac{\sum_{j=1}^{n} q_j}{\sum_{j=1}^{n} \left(T_{s,in,j} - T_{s,out,j} \right)} \quad \left[\mathrm{W} / \mathrm{m}^2 \mathrm{K} \right] \tag{4}$$

$$U = \frac{1}{R_{tot}} = \frac{1}{R_{s,int} + R_{cond} + R_{s,ext}} \quad \left[\mathrm{W}/\mathrm{m^2K}\right] \tag{5}$$

where:

- Λ is the thermal conductance;
- U is the thermal transmittance;
- $\sum_{j=1}^{n}\left(T_{s,in,j} - T_{s,out,j}\right)$ is the progressive sum of the differences between internal and external surface temperatures;
- $\sum_{j=1}^{n} q_j$ is the progressive sum of the density of the heat flux;
- R_{cond} is the conduction resistance.
- $R_{s,int}$ and $R_{s,ext}$ are the internal and external surface thermal resistances;
- R_{tot} is the total thermal resistance.

The experimental study of the blocks also employed the IRT technique to assess the thermal distribution on the external surface of the blocks. Thermal images were captured by positioning the thermal camera at a distance of 1.5 m from the samples. The configurations utilized for acquiring thermal images are depicted in Fig. 14.

The instruments utilized for the experimental analyses are shown in Table 2.

3.5. Uncertainty analysis

The uncertainty analysis of the measured data was carried out following the Holman's method [45], as shown by Eq. (6) [45]:

$$W_U = \left[\left(\frac{\partial U}{x_1}\cdot w_1\right)^2 + \left(\frac{\partial U}{x_2}\cdot w_2\right)^2 + \ldots + \left(\frac{\partial U}{x_n}\cdot w_n\right)^2\right]^{1/2} \tag{6}$$

where:

- W_U is the uncertainty in the transmittance value calculated;
- w_1, w_2, …, w_n are the uncertainties in the independent variables x_1, x_2, …, x_n, given by technical data sheets.

4. Results and discussion

The tests conducted using the HFM method yielded the determination of the thermal transmittance for the three blocks. Table 3 shows the average values of heat flux (q_{ave}), internal ($T_{s,int,ave}$) and external ($T_{s,ext,ave}$) surface temperatures for each experimental campaign carried out.

The graphs in Fig. 15 highlight the values of heat flux (instantaneous and averaged) and internal and external surface temperatures (instantaneous) of the last 24 h of measurements for each block.

Fig. 16 illustrates the trends of transmittance and their convergence values.

It is worth noting that the honeycomb block (Block 3) exhibits the best performance, with a thermal transmittance of 1.08 ± 0.04 W/m^2K. This is followed by the block featuring hexagonal cells without vertical partitions, oriented horizontally (Block 1b) with a thermal transmittance of 1.13 ± 0.04 W/m^2K. Conversely, the block with hexagonal cells without horizontal partitions, oriented vertically (Block 1a), demonstrates the poorest thermal performance, with a thermal transmittance of 1.22 ± 0.04 W/m^2K.

Table 4 compares the U-values obtained with the configurations analyzed, highlighting the percentage difference compared to the results obtained for Block 1a. The data indicate that the thermal transmittance obtained for Block 3 was 11.5 % lower than the value obtained for Block 1a. This result underscores the effectiveness of the insertion of horizontal partitions and the vertical translation of

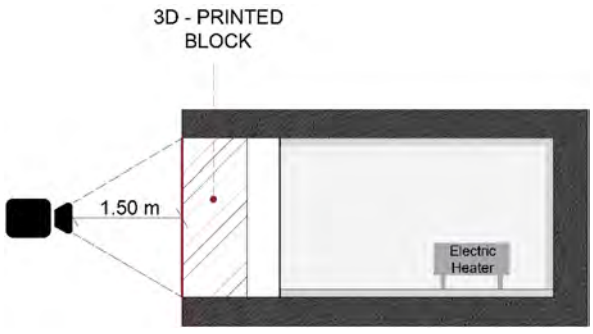

Fig. 14. Schematic representation of the thermographic survey.

Table 2
Technical specifications of the measuring instruments employed for the experimental analyses.

Sensor	Type	Measuring Range	Sensitivity
Heat flow meter	Hukseflux HFP01	From −2000 to 2000 W/m^2	60 × 10^{-6} V/(W/m^2)
Surface temperature	LSI Lastem DLE 124	From −40 to 80 °C	0.01 °C
Air Temperature	LSI Lastem DLA 033	From −40 to 80 °C	0.01 °C
Datalogger	LSI Lastem M-Log ELO008	From −300 to 1200 mV	40 μV
IR camera	FLIR T1020	From −40 to 2000 °C	1024 × 728 pixel

Table 3
Average of the experimental values recorded for each test.

Tests	Block	q_{ave} [W/m^2]	$T_{s,int,ave}$ [K]	$T_{s,ext,ave}$ [K]
Test 1	Block 1a	30.6 ± 0.9	45.8 ± 0.1	25.2 ± 0.1
Test 2	Block 1b	29.6 ± 0.9	46.5 ± 0.1	25.6 ± 0.1
Test 3	Block 2	30.8 ± 0.9	46.6 ± 0.1	25.8 ± 0.1
Test 4	Block 3	27.8 ± 0.8	46.1 ± 0.1	25.1 ± 0.1

the cells in reducing the heat flow passing through the block.

The obtained results demonstrate what is described in Section 3.1 regarding the "Theoretical Background," namely that:

- increasing the geometric complexity of the block attenuates thermal conduction through PLA, increasing thermal resistance;
- by varying the aspect ratio (H/L) and, in particular, the characteristic length (H), the Rayleigh number is modified, consequently affecting the Nusselt number. However, the results show that the block with reduced (H) (i.e., Block 2) is only marginally better than Block 1a. For a singular cavity, it is known [39] that reducing the ratio (L/H) reduces *Nu*. The difference in this case is most probably due to the mutual interference of the multicellular structure.
- considering the previous point, the best performance given by Block 3 is mostly due to the increased geometry complexity.

Once stable and steady thermal conditions were achieved (i.e., at the conclusion of the 24 h of heat flux measurements), thermal images were captured. The thermal images in Fig. 17 display the thermal distributions on the external surfaces of the considered blocks.

Thermal images highlight the internal structure of the blocks, revealing the varied cavity configurations and internal thermal stratifications resulting from convective fluid motions. It's worth noting that in Block 3, the thermal distribution is significantly more homogeneous. Additionally, the air cavities reach lower temperatures. In contrast, Block 2, despite its horizontal partitions, shows considerable vertical thermal stratification.

5. Conclusions

This study investigated the thermal behavior of three 3D-printed blocks with similar geometries, featuring hexagonal cells, but differing in complexity due to the inclusion of horizontal partitions and vertical translation of the cells. The research aimed to experimentally quantify how variations in the orientation and size of air cavities affect heat flow through the blocks. The experimental analysis, employing the Hot Box, Heat Flow Meter (HFM) method, and Infrared Thermography (IRT) technique, was conducted under identical steady-state conditions for all three blocks. The main innovations of this study include the utilization of 3D printing technology to fabricate blocks with intricate internal geometries aimed at minimizing heat transfer, as well as the development of a tailored experimental setup to assess the thermal performance of these blocks.

The main findings of the study are summarized below:

- The variation in the orientation of the air cavities in Block 1 facilitated the quantification of their impact on heat transfer. The thermal transmittance was measured to be 1.22 ± 0.04 W/m^{2}K for the block with vertical cavities (Block 1a) and 1.13 ± 0.04 W/m^{2}K for the block with horizontal cavities (Block 1b), representing a decrease of 7.4 %.
- The inclusion of three horizontal partitions in Block 2 led to a marginal improvement in performance compared to Block 1a, with a thermal transmittance 3.3 % lower, measured at 1.18 ± 0.04 W/m^{2}K. However, Block 2 exhibited slightly inferior performance compared to Block 1b, with a thermal transmittance 4.4 % higher.
- The honeycomb-inspired block design, featuring three internal partitions and vertical translation of the cells, exhibited the best thermal performance among all tested blocks. It achieved a transmittance of 1.08 ± 0.04 W/m^{2}K, representing an 11.5 % reduction compared to the transmittance of the baseline block (Block 1a).
- The IRT technique facilitated the assessment of thermal distribution on the outer surface of the blocks with various configurations. As a result, the effects of the geometric configurations of the cavities on fluid motion could be observed. Block 3 showed the most homogeneous surface thermal distribution.

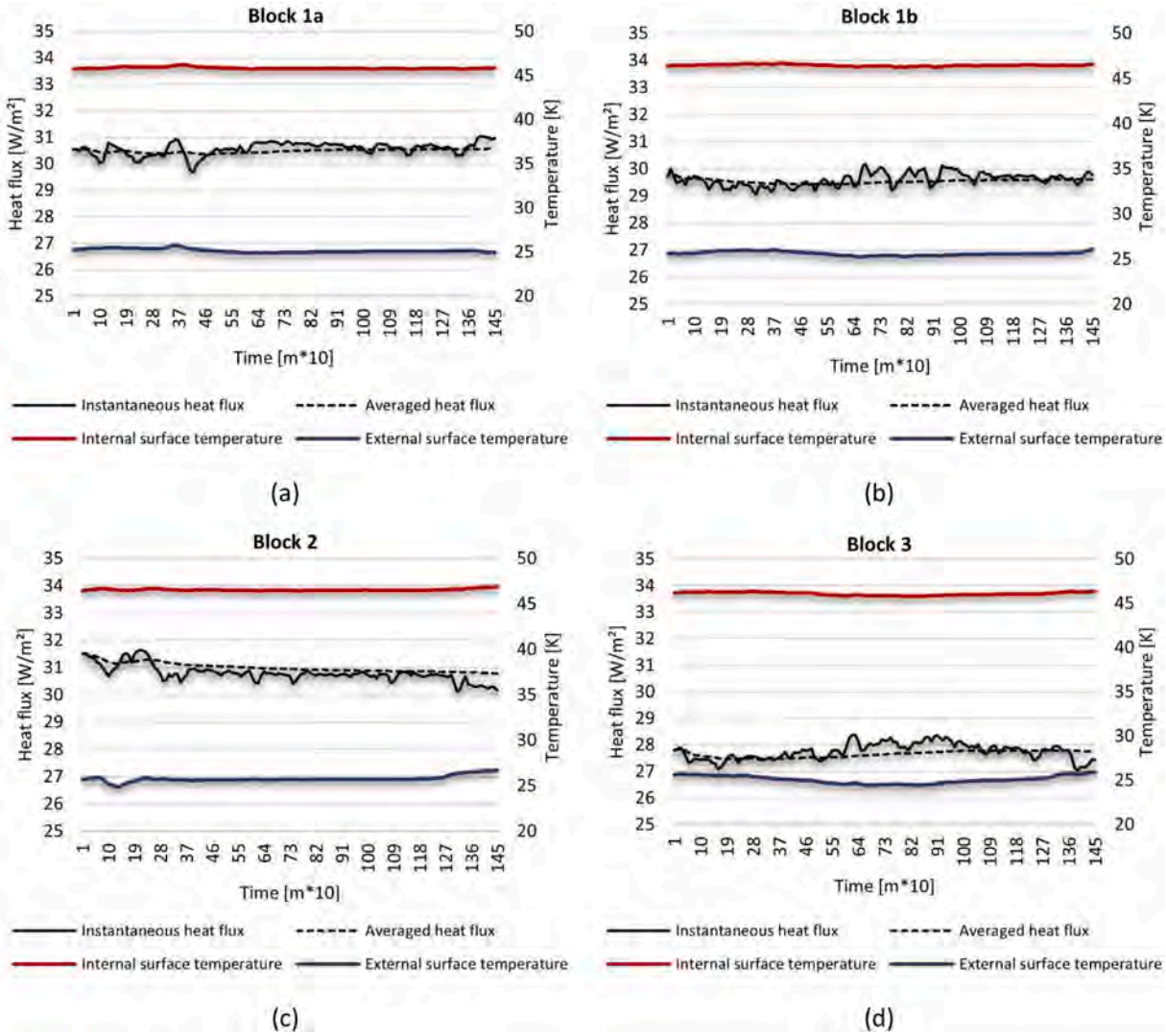

Fig. 15. Measured experimental data. (a) Block 1a. (b) Block 1b. (c) Block 2. (d) Block 3. *Legend*: Continuous black line represents the instantaneous heat flux; Dashed black line represents the averaged heat flux; Red line is the internal surface temperature; Blue line is the external surface temperature. (For interpretation of the references to colour in this figure legend, the reader is referred to the Web version of this article.)

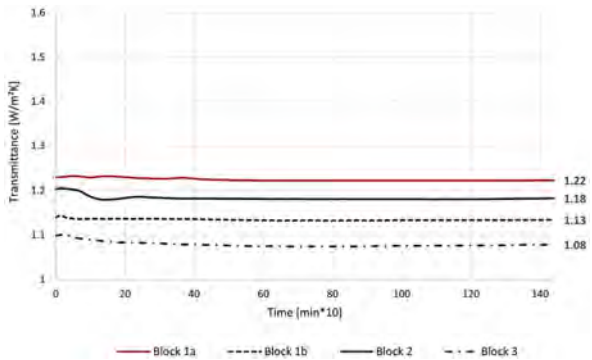

Fig. 16. Trends of transmittance and their convergence values.

Table 4
Comparison between the U-values of the blocks (values in [W/m^{2}K]).

Block type	U	Percentage difference[a]
Block 1a	1.22 ± 0.04	–
Block 1b	1.13 ± 0.04	−7.4 %
Block 2	1.18 ± 0.04	−3.3 %
Block 3	1.08 ± 0.04	−11.5 %

[a] with respect to Blockptablefo 1a.

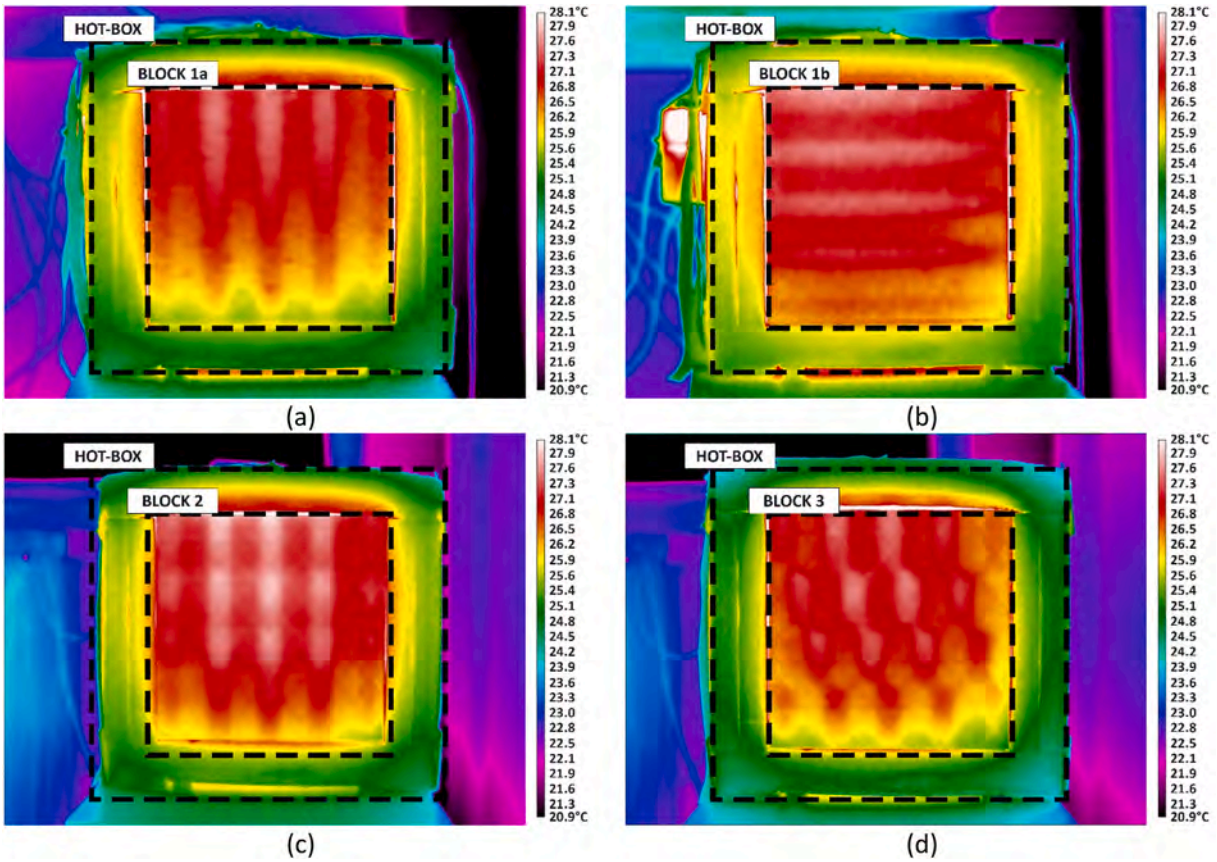

Fig. 17. Thermal images of the samples. Thermal distribution on the external surface of the blocks. (a) Block 1a. (b) Block 1b. (c) Block 2. (d) Block 3.

The study underscores the capabilities of 3D printing in creating blocks with intricate geometries, opening avenues for further exploration in thermal optimization and the design of structures capable of mitigating heat flux.

Moreover, the construction of nature-inspired envelope components, known as biomimetic architecture, has demonstrated energy benefits for building design. In this context, 3D printing emerges as a promising tool for constructing buildings inspired by nature.

Future developments of this work will focus on investigating geometrically complex structures with the aim of further optimizing the energy performance of a building's envelope.

Funding

This research received no external funding.

Nomenclature

Abbreviations			
3DP	3D printing	U	Thermal transmittance, W/m^{2}K
		v	Kinematic viscosity, m^2/s

(*continued on next page*)

(*continued*)

3DPC	3D-printed concrete	W	Uncertainty in the calculated value
AM	Additive manufacturing		
CHSs	Cement-based honeycomb structures	*Greek symbols*	
FEM	Finite element model	α	Thermal diffusivity, m^2/s
GHG	Greenhouse gas	β	Volume expansion coefficient [1/K]
HFM	Heat-flow meter	Λ	Conductance, W/m^2K
IRT	IRT	λ	Thermal Conductivity, W/mK
Nu	Nusselt number		
PLA	Polylactic acid	*Subscripts*	
Pr	Prandtl number	ave	Average
Ra	Rayleigh number	c	cold
		conv	Convective
		cond	Conduction
Roman symbols		eff	Effective
g	Gravitational acceleration, m/s^2	ext	External
H	Enclosure height, m	hot	Hot
L	Dimension of the cavity in the main direction of the flow, m	in	Indoor
		int	Internal
q	Heat flux, W/m^2	j	j-th
R	Thermal resistance, m^2K/W	n	n-th
s	Thickness, m	out	Outdoor
T	Temperature, °C or K	s	Surface
		tot	Total

CRediT authorship contribution statement

Tullio de Rubeis: Writing – review & editing, Writing – original draft, Supervision, Resources, Methodology, Investigation, Formal analysis, Data curation, Conceptualization. **Annamaria Ciccozzi:** Writing – original draft, Resources, Investigation, Data curation. **Domenica Paoletti:** Writing – review & editing, Supervision. **Dario Ambrosini:** Writing – review & editing, Supervision, Methodology, Formal analysis, Data curation.

Declaration of competing interest

The authors declare that they have no known competing financial interests or personal relationships that could have appeared to influence the work reported in this paper.

References

[1] Energy efficiency in buildings. Available online: https://commission.europa.eu/news/focus-energy-efficiency-buildings-2020-02-17_en (accessed on 7 February 2023).
[2] European Green Deal. Available online: https://commission.europa.eu/strategy-and-policy/priorities-2019-2024/european-green-deal_it (accessed on 7 February 2023).
[3] M. Muttillo, I. Nardi, V. Stornelli, T. de Rubeis, G. Pasqualoni, D. Ambrosini, On field infrared thermography sensing for PV system efficiency assessment: results and Comparison with electrical models, Sensors 20 (February 2020) 1055.
[4] T. Wangler, N. Roussel, F.B. Bos, T.A.M. Salet, R.J. Flatt, Digital concrete: a review, Cement Concr. Res. 123 (September 2019) 105780.
[5] A. Nadal, J. Pavón, O. Liébana, 3D printing for construction: a procedural and material-based approach, Inf. Construcción 69 (546) (2017). April-June.
[6] S.C. Renjith, K. Park, G.E. Okudan Kremer, A design framework for Additive manufacturing: Integration of additive manufacturing capabilities in the early design process, Int. J. Precis. Eng. Manuf. 21 (October 2019) 329–345.
[7] U. Chadha, A. Abrol, N. Paras, V. Agastya Tiwari, S. Kirubaa Shanker, S. Kumaran Selvaraj, Performance evaluation of 3D printing technologies: a review, recent advances, current challenges, and future directions, Progress in Additive Manufacturing 7 (February 2022) 853–886.
[8] A.S.J. Suiker, Mechanical performance of wall structures in 3D printing processes: theory, design tools and experiments, Int. J. Mech. Sci. 137 (March 2018) 145–170.
[9] S. Rouf, A. Raina, M.I. Ul Haq, N. Naveed, S. Jeganmohan, A.F. Kichloo, 3D printed parts and mechanical properties: influencing parameters, sustainability aspects, global market scenario, challenges and applications, Advanced Industrial and Engineering Polymer Research 5 (July 2022) 145–158.
[10] B. Panda, S.C. Paul, L.J. Hui, Y.W.D. Tay, M.J. Tan, Additive manufacturing of geopolymer for sustainable built environment, J. Clean. Prod. 167 (November 2017) 281–288.
[11] H. Sozer, Improving energy efficiency through the design of the building envelope, Build. Environ. 45 (December 2010) 2581–2593.
[12] S. Lorente, M. Petit, R. Javelas, Simplified analytical model f or thermal transfer in vertical hollow brick, Energy Build. 24 (July 1996) 95–103.
[13] P. Stefanizzi, A. Lippolis, S. Liuzzi, Experimental and numerical analysis of heat transfer in the cavities of hollow blocks, Int. J. Heat Technol. 31 (2013) 149–154.
[14] W. Hu, Y. Xia, F. Li, H. Yu, C. Hou, X. Meng, Effect of the filling position and filling rate of the insulation material on the insulation performance of the hollow block, Case Stud. Therm. Eng. 26 (August 2021) 101023.
[15] A.S. Al-Tamimi, O.S.B. Al-Amoudi, M.A. Al-Osta, M.R. Ali, A. Ahmad, Effect of insulation materials and cavity layout on heat transfer of concrete masonry hollow blocks, Constr. Build. Mater. 254 (September 2020) 119300.
[16] T. Suntharalingam, I. Upasiri, P. Gatheeshgar, K. Poologanathan, B. Nagaratnam, P. Santos, H. Rajanayagam, Energy performance of 3D-printed ConcreteWalls: a numerical study, Buildings 11 (September 2021) 432.
[17] Q. Zhang, X. Yang, P. Li, G. Huang, S. Feng, C. Shen, B. Han, X. Zhang, F. Jin, F. Xu, T. Jian Lu, Bioinspired engineering of honeycomb structure – using nature to inspire human innovation, Prog. Mater. Sci. 74 (October 2015) 332–400.

[18] T. de Rubeis, A. Ciccozzi, L. Giusti, D. Ambrosini, The 3D printing potential for heat flow optimization - influence of block geometries on heat transfer processes, Sustainability 14 (23) (November 2022) 15830.
[19] G. Zhu, H. Jing, J. Wu, S. Chen, Y. Gao, Q. Yin, Z. Yu, Y. Qiao, J. Ren, Study on heat transfer characteristics of cement-based honeycomb structures based on infrared imaging, J. Build. Eng. 68 (June 2023) 106134.
[20] T. de Rubeis, 3D-Printed blocks: thermal performance analysis and opportunities for insulating materials, Sustainability 14 (January 2022) 1077.
[21] T. de Rubeis, A. Ciccozzi, G. Pasqualoni, D. Paoletti, D. Ambrosini, On the use ofWaste materials for thermal improvement of 3D-printed block—an experimental Comparison, Buildings 13 (1136) (April 2023).
[22] T. de Rubeis, A. Ciccozzi, G. Pasqualoni, D. Paoletti, D. Ambrosini, " Thermal optimization of 3D-printed block – hot Box and heat flow meter experimental analysis,", in: 2023 8th International Conference on Smart and Sustainable Technologies (SpliTech)., IEEE, 2023, pp. 1–5.
[23] M.V. Sarakinioti, M. Turrin, T. Konstantinou, M. Tenpierik, U. Knaack, Developing an integrated 3D-printed façade with complex geometries for active temperature control, Mater. Today Commun. 15 (June 2018) 275–279.
[24] A. Mihalache, A. Hriţuc, M. Boca, B. Oroian, I. Condrea, C. Botezatu, L. Slătineanu, Thermal insulation capacity of a 3D printed material, Macromol 396 (April 2021) 1–4.
[25] B. Grabowska, J. Kasperski, The thermal conductivity of 3D printed plastic insulation materials—the effect of optimizing the regular structure of closures, Mater 13 (October 2020) 2–15.
[26] D. Dey, B. Panda, An experimental study of thermal performance of 3D printed concrete slabs, Mater. Lett. 330 (January 2023) 133273.
[27] M. Kaszynka, N. Olczyk, M. Techman, S. Skibicki, A. Zielinski, K. Filipowicz, T. Wroblewski, M. Hoffmann, Thermal-humidity parameters of 3D printed wall, IOP Conf. Ser. Mater. Sci. Eng. 471 (2019) 1–9.
[28] A. Alkhalidi, D. Hatuqay, Energy efficient 3D printed buildings: material and techniques selection worldwide study, J. Build. Eng. 30 (July 2020) 1–13.
[29] H. Marais, H. Christen, S. Cho, W. De Villiers, G. Van Zijl, Computational assessment of thermal performance of 3D printed concrete wall structures with cavities, J. Build. Eng. 41 (September 2021) 1–21.
[30] D. Nemova, E. Kotov, D. Andreeva, S. Khorobrov, V. Olshevskiy, I. Vasileva, D. Zaborova, T. Musorina, Experimental study on the thermal performance of 3D-printed enclosing structures, Energies 15 (June 2022) 1–22.
[31] T. Suntharalingam, I. Upasiri, P. Gatheeshgar, K. Poologanathan, B. Nagaratnam, P. Santos, H. Rajanayagam, Energy performance of 3D-printed ConcreteWalls: a numerical study, Buildings 11 (432) (September 2021).
[32] K. Cuevas, J. Strzałkowski, J.S. Kim, C. Ehm, T. Glotz, M. Chougan, S.H. Ghaffar, D. Stephan, P. Sikora, Towards development of sustainable lightweight 3D printed wall building envelopes – experimental and numerical studies, Case Stud. Constr. Mater. 18 (February 2023) E01945.
[33] Y. He, Y. Zhang, C. Zhang, H. Zhou, Energy-saving potential of 3D printed concrete building with integrated living wall, Energy Build. 222 (May 2020) 110110.
[34] D. El-Mahdy, H.S. Gabr, S. Abdelmohsen, SaltBlock as a 3D printed sustainable construction material in hot arid climates, J. Build. Eng. 43 (November 2021) 103134.
[35] G. Atakok, M. Kam, H.B. Koc, Tensile, three-point bending and impact strength of 3D printed parts using PLA and recycled PLA filaments: a statistical investigation, J. Mater. Res. Technol. 18 (2022) 1542–1554. May–June.
[36] O. Menezes, T. Roberts, G. Motta, M.H. Patrenos, W. McCurdy, A. Alotaibi, M. Vanderpool, M. Vaseghi, A. Beheshti, K. Davami, Performance of additively manufactured polylactic acid (PLA) in prolonged marine environments, Polym. Degrad. Stab. 199 (May 2022) 109903.
[37] S.L. Rodríguez-Reyna, C. Mata, J.H. Díaz-Aguilera, H.R. Acevedo-Parra, F. Tapia, Mechanical properties optimization for PLA, ABS and Nylon + CF manufactured by 3D FDM printing, Mater. Today Commun. 33 (December 2022) 104774.
[38] W.H. Rohsenow, J.P. Hartnett, Y.I. Cho (Eds.), Handbook of Heat Transfer, third ed., McGraw-Hill, 1998.
[39] A. Bejan, Convection Heat Transfer, second ed., Wiley, New York, 1995. Ch. 5.
[40] The mathematics of the honeycomb, Sci. Digest (June 1985) 74–77.
[41] D. Andréen, R. Soar, Termite-inspired metamaterials for flow-active building envelopes, Front. Mater. 10 (May 2023) 1126974.
[42] K.V. Frish, Nel Mondo Delle Api, vol. 2, 1984. Edagricole, Bologna.
[43] EN ISO 9869-1:2014; Thermal Insulation—Building Elements—In-Situ Measurement of Thermal Resistance and Thermal Transmittance, Part 1: Heat Flow Meter Method, European Committee for Standardization, Brussels, Belgium, 2014.
[44] EN ISO 6946:2017; Building Components and Building Elements—Thermal Resistance and Thermal Transmittance—Calculation Methods, European Committee for Standardization, Brussels, Belgium, 2017.
[45] J.P. Holman, Experimental Methods for Engineers, eighth ed., McGraw-Hill Series in Mechanical Engineering; McGraw-Hill, New York, NY, USA, 2012. ISBN 13: 9780073529301.